Nanowires self-assembling β-MnO_2 nanospheres to form cross-linking 3D hierarchical porous networks: template-free fabrication and good supercapacitive performance at a broad temperature

Li-Li Yu[a*], Wei-Ling Xu[a], Jian-Guo Zhang[a], Shuang Li[a], Rong-Bing Li[a], Jing-Tai Zhao[b]

[a] *School of Material Science and Engineering, Shanghai University, Shanghai, 200444, P.R. China*

[b] *School of Materials Science and Engineering, Guilin University of Electronic Technology, Guilin 541004, China*

Correspond to: lly522@shu.edu.cn

Table S1 molar ratio, productivity of as-prepared β-MnO_2

Sample	1,3-butanediol /$KMnO_4$[a]	yield [%]
S-1	0.5	~85
S_{CPS}	0.8	~97.7
S-2	1.2	~94

a- Molar ratio, the use of $KMnO_4$ is the same in all samples;

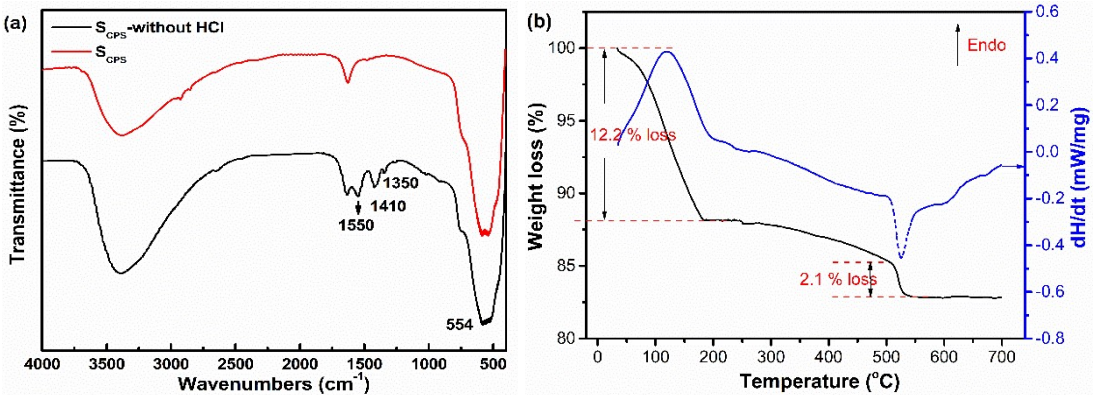

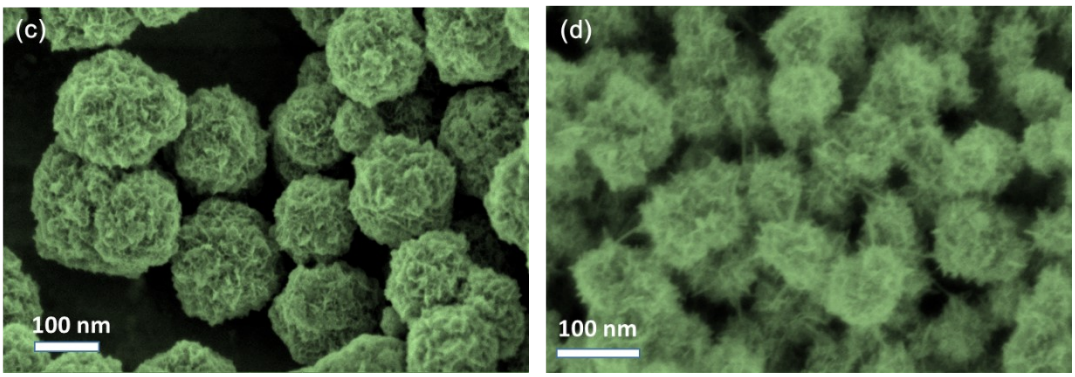

Fig. S1. IR spectra (a) of samples S_{CPS} and S_{CPS}-without HCl, and TG TG-DSC curves (b) of sample S_{CPS}. And SEM images of sample S-1 (c) and S-2 (d)

As shown in Fig. S1a, compared to sample $S_{CPS,}$ peaks centered at 1550 cm^{-1}, 1410 cm^{-1}, 1350 cm^{-1}, assigned to the COO- antisymmetric and symmetric stretching vibrations, and O-H stretching vibrations of suspended hydroxyl, are clearly seen in the IR spectrum of sample S_{CPS} before washed by 0.5 M hydrochloric (named as S_{CPS}-without HCl), suggesting the formation of some by-product of organic salt [1], which can solute in hydrochloric.

As shown in Fig. S1b, only two weight loss ~12.2% and ~2.1% with two exothermic peaks (around 130°C and 520°C) are detected. The former can be attributed to the evaporation of the physical absorbed water, and the latter is derived from the phase transformation from MnO_2 to Mn_2O_3, which is proved by our previous literatures [2, 3]. In addition, no other endo/exothermic peaks are detected in temperature region of 210~520°C, suggesting that no other chemical reaction happens in the heat process from room temperature to 500°C in air.

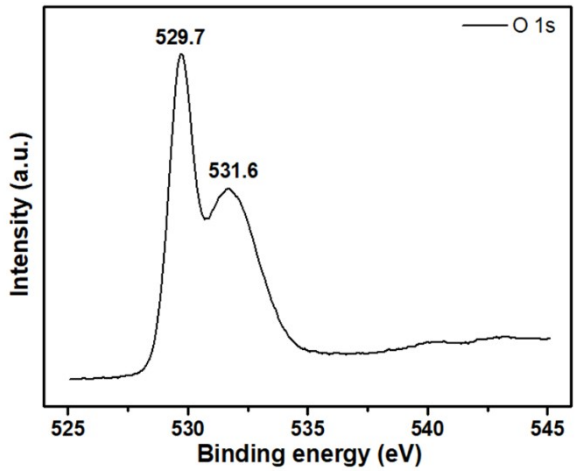

Fig. S2 O 1s spectrum of sample S_{CPS}

As shown in Fig. S2, peaks centred at 529.7 and 531.6 eV of O 1s are atributed to the Mn−O−Mn and Mn−OH groups [4], respectively.

S1. Electrode preparation and measurement

Working electrodes are constructed by mixing the active material (as-synthesized β-MnO_2, carbon black and polyvinylidene fluoride (PVDF) in a mass ratio of 8:1:1. Typically, the mixtures were formed into slurries first by adding a small amount of 1-methyl-2-pyrrolidinone solutions. And then the prepared slurries were coated onto a stainless steel grid with an apparent area of 1×1 cm^2, and dried in vacuum at 80°C for 12 h. Finally, the dried electrodes are pressed under 10 MPa.

For three-electrode, platinum sheet (99.99%), Ag/AgCl cell (in 3 M KCl solution) are selected as counter and reference electrodes, respectively. CV data were collected in 0-0.9 V *vs.* Ag/AgCl in a scan rate range of 2-100 mV s^{-1}. The EIS were measured in a frequency range of 10^5-10^{-2} Hz using an alternating current bias of 5 mV s^{-1}. GCDs were evaluated at current densities from 0.5 A g^{-1} to 20 A g^{-1}. For two-electrode cell, an asymmetric capacitor MnO_2//AC (activated carbon, purchased by Sinopharm Chemical Reagent Co., Ltd) were assembled and evaluated by CV and GCD in a voltage window of 1.7 V as well, in considering of the stabilities of active materials in working temperature of 5-80 °C. The mass ratio of AC and S-2 was 1.4 calculated by Equation (1) according to the charge balance theory.

$$\frac{m_+}{m_-} = \frac{C_- \Delta V_-}{C_+ \Delta V_+} \quad (1)$$

where C_+ and C_-, ΔV_+ and ΔV_- represent the specific capacitance and the potential window of positive and negative electrodes, respectively.

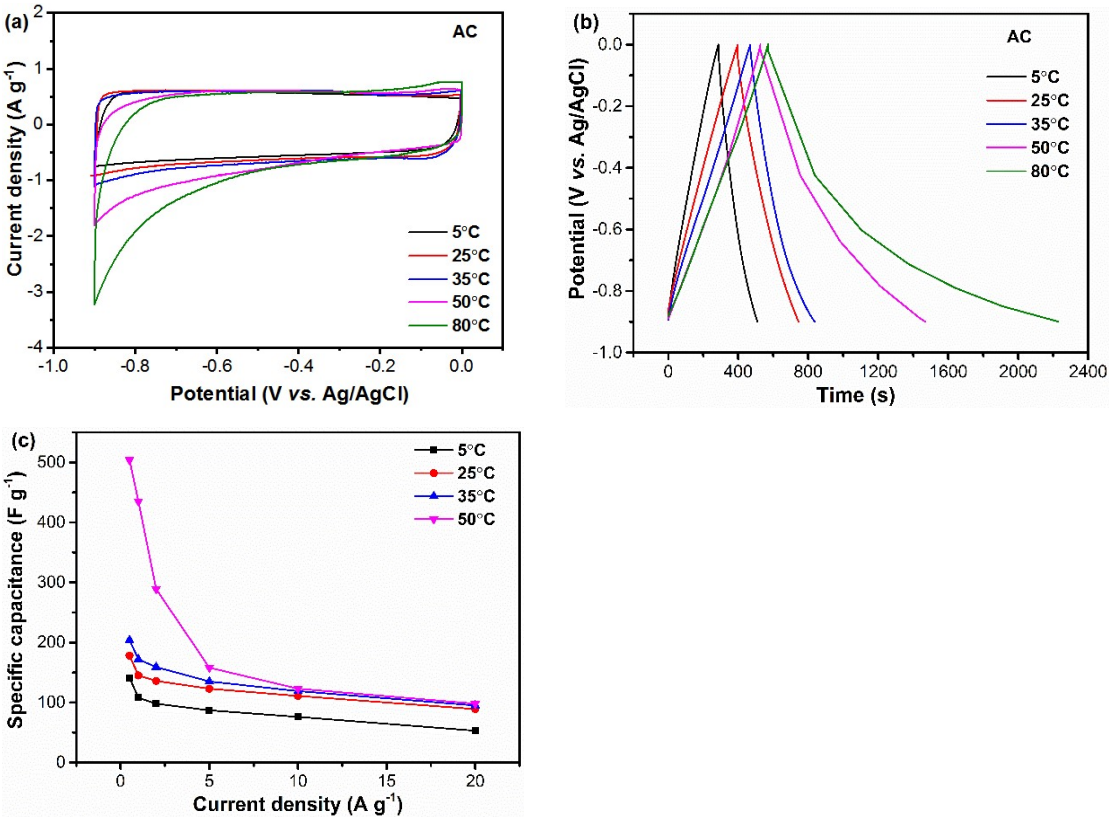

Fig. S3. CV curves at 5 mV s^{-1} scan rate (a), GCD at a current density of 0.5 A g^{-1} (b), specific capacitance *vs*. charge/discharge current densities of 0.5-20 A g^{-1} (c) of commercial active carbon at different working temperature (5-80°C).

Fig.S3a shows the CV curves of commercial activated carbon (AC) in different temperatures at a scan rate of 5 mV s^{-1}. It is noted that the CV curves of AC become asymmetry above 50°C due to the hydrogen evolution. This is in accordance with the GCD data. As shown in Fig. S3b, the ideal symmetrical rectangle become asymmetric as the operation temperature is above 35°C. These data suggest that the commercial AC can only working at temperatures of 5-35°C. This is supported by its rate capability. As shown in Fig. S3c, different from those at 5-35°C, the specific capacitance of AC at 50°C decrease dramatically as the current density increasing from 0.5 A g^{-1} to 5 A g^{-1}, and then become constant, demonstrating its poor rate capability at temperature above

35°C.

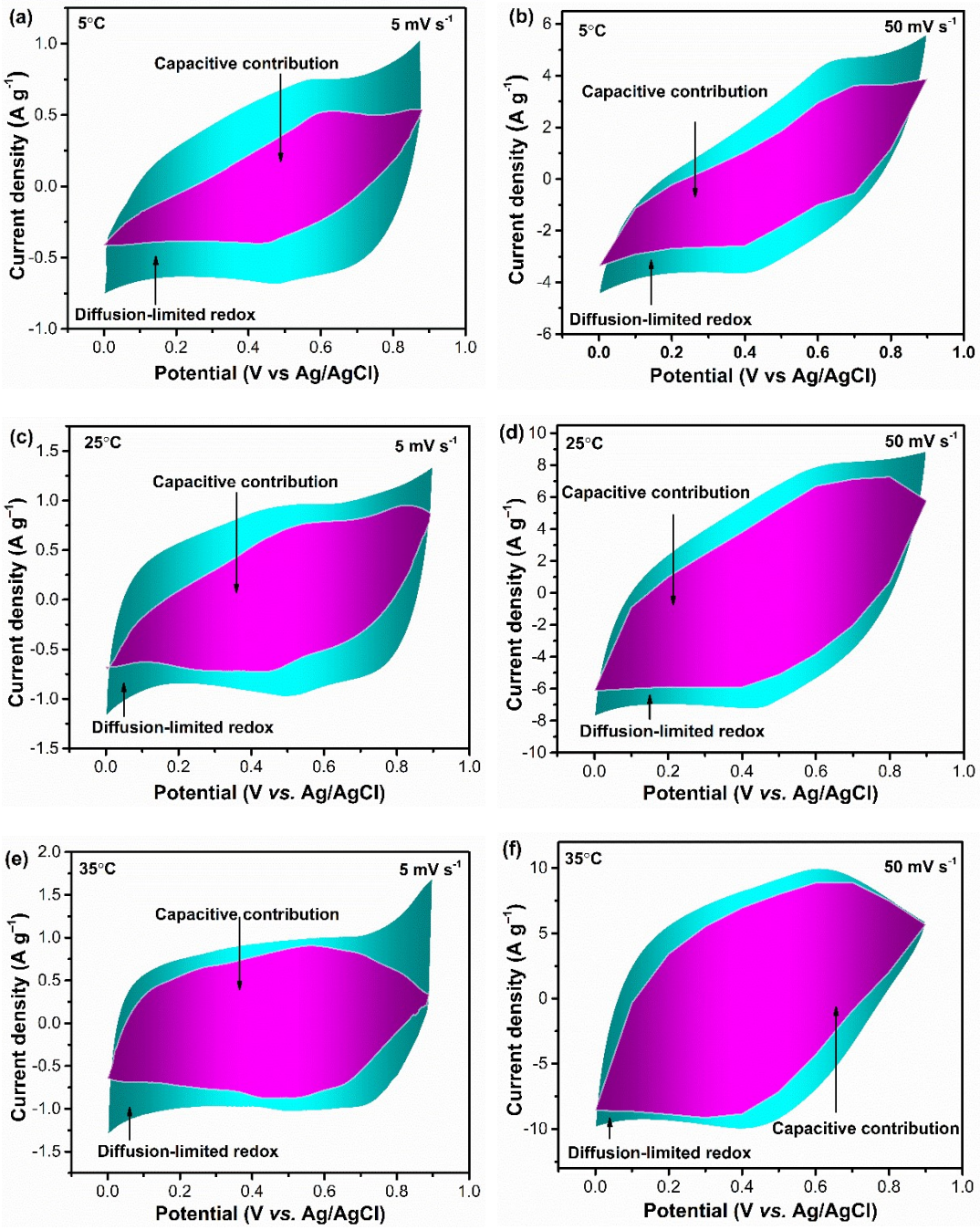
(a)
5°C
5 mV s-1
Capacitive contribution
Diffusion-limited redox
Current density (A g-1)
Potential (V vs Ag/AgCl)
(b)
5°C
50 mV s-1
Capacitive contribution
Diffusion-limited redox
Current density (A g-1)
Potential (V vs Ag/AgCl)
(c)
25°C
5 mV s-1
Capacitive contribution
Diffusion-limited redox
Current density (A g-1)
Potential (V vs. Ag/AgCl)
(d)
25°C
50 mV s-1
Capacitive contribution
Diffusion-limited redox
Current density (A g-1)
Potential (V vs. Ag/AgCl)
(e)
35°C
5 mV s-1
Capacitive contribution
Diffusion-limited redox
Current density (A g-1)
Potential (V vs. Ag/AgCl)
(f)
35°C
50 mV s-1
Capacitive contribution
Diffusion-limited redox
Current density (A g-1)
Potential (V vs. Ag/AgCl)

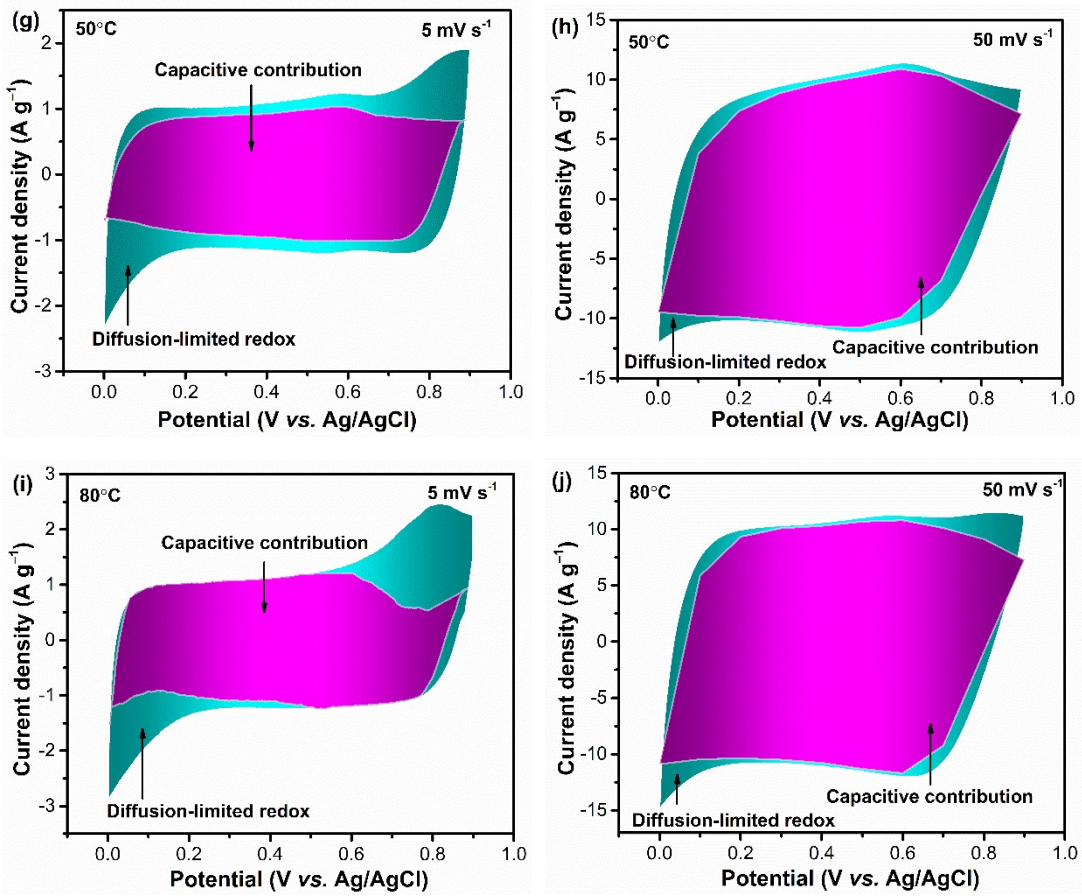

Fig.S4 Surface-controlled and diffusion-controlled capacitances of electrode S_{CPS} working at different temperatures (5-80°C) at scan rates of 5 mV s^{-1} (a, c, e, g, i) and 50 mV s^{-1} (b, d, f, h, j), respectively.

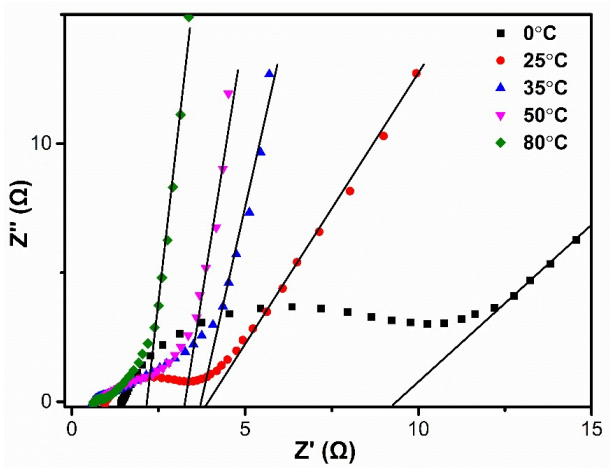

Fig. S5 The equivalent series resistances (ESRs) of electrode S_{CPS}.

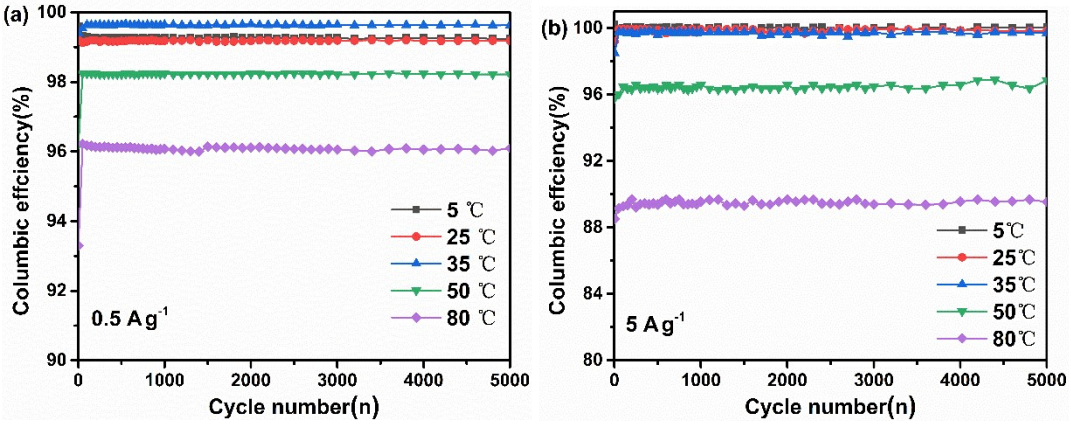

Fig. S6 The coulomb efficiencies of electrode S_{CPS} at 0.5 (a) and 5 (b) A g^{-1} after 5000 cycles at working temperatures of 5-80 °C.

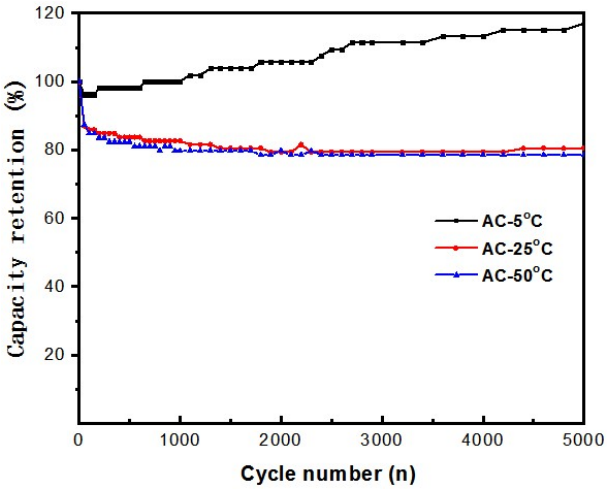

Fig.S7 Cycle performance of AC after 5000 cycles at 5 A g^{-1}in different working temperatures.

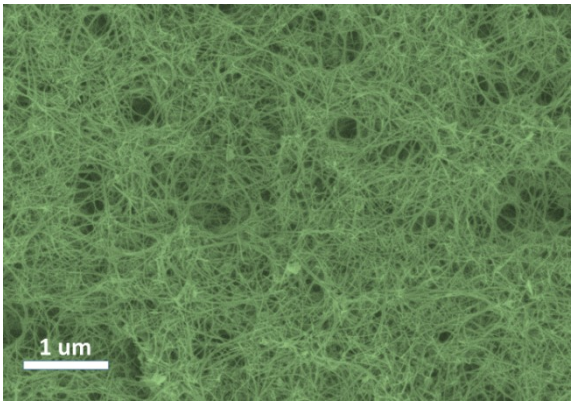

Fig. S8 SEM image of as-prepared electrode S_{CPS} after 5000 cycles at 5 A g^{-1} working at 80°C.

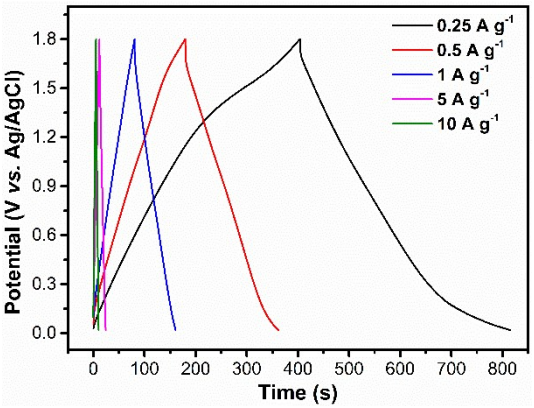

Fig.S9 GCD curves of S_{CPS}//AC capacitor working at 25°C.

Table S2. The fitted impedance parameters of samples S_{CPS} at different operation temperatures.

T(°C)	R_s(Ω)	R_{ct}(Ω)	W(Ω $s^{-1/2}$)
5	1.46	8.59	9.43
25	0.99	4.28	5.06
35	0.70	3.22	2.47
50	0.62	3.09	1.16
80	0.60	2.83	1.14

Table S3. The equivalent series resistances (ESRs) estimated from the intercept of the low frequency impendence spectrum with the real axis of S_{CPS} at different working temperatures.

Test temperature(°C)	Equivalent series resistance (ESR)
5	9.25
25	3.86
35	3.67
50	3.26
80	2.15

Reference

[1] Z. Niu, J. Chen, H. H. Hng, J. Ma, X. Chen, A leavening strategy to prepare reduced graphene oxide foams[J]. Adv. Mater. 2012, **24**(30): 4144-50.

[2] L.L. Yu, J. Zhu, J.T. Zhao, Beta-manganese dioxide nanoflowers self-assembled by ultrathin nanoplates with enhanced supercapacitive performance[J]. J. Mater. Chem. A 2014, **2**(24): 9353-60.

[3] R. Li, L.L. Yu, S. Li, J. Fan, R. Luo, J.T. Zhao, Facile synthesis of hierarchical mesoporous beta-manganese dioxide nanoflowers with extremely high specific surface areas for high-performance electrochemical capacitors[J]. Electrochim. Acta 2018, **284**: 52-9.

[4] D. P. Dubal, R. Holze, Self-assembly of stacked layers of Mn_3O_4 nanosheets using a scalable chemical strategy for enhanced, flexible, electrochemical energy storage[J]. J. Power Sources 2013, **238**: 274−282.